Synchronous Change of Atmospheric CO_2 and Antarctic Temperature During the Last Deglacial Warming

F. Parrenin *et al.*

Science **339**, 1060 (2013);
DOI: 10.1126/science.1226368

Science (print ISSN 0036-8075; online ISSN 1095-9203) is published weekly, except the last week in December, by the American Association for the Advancement of Science, 1200 New York Avenue NW, Washington, DC 20005.

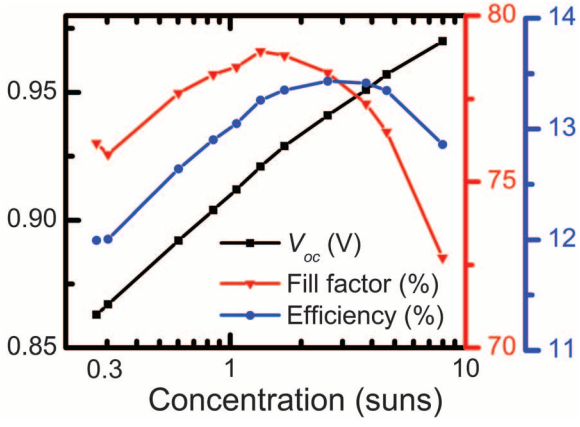

Fig. 4. Characterization of cell from sample E under concentrated illumination.

effects such as surface pinning (*26*). Additional experiments are needed to understand the high V_{oc}.

Because multijunction III-V PV is currently being deployed for concentrator PV—where large-area, low-cost optics are used to collect sunlight and focus it onto small, high-performance solar cells—we have also investigated the performance of the cell with highest V_{oc} (sample E) under concentration (Fig. 4). The V_{oc} increases logarithmically as expected up to 0.97 V. However, the fill factor decreases, which indicates a series resistance, possibly originating from the TCO or the small contact area of the NW tips. The efficiency under concentrated illumination for this cell therefore peaks at 13.4% at 2.6 suns. The angular dependence, which is important for diffuse light conditions, has not been investigated experimentally, but previous simulations have indicated weak angular dependence up to 40° (*12*).

Lastly, we assess the technical maturity of our design. We fabricated seven working cells on the same sample (average efficiency of 12.0% with standard deviation of 1.4%) and reproduced similar results in separate growth and processing batches. The best sample was stored 2 months in ambient air before the measurement, and the degradation in absolute efficiency of somewhat older samples is less than 0.5% over a period of 6 months. This design should be readily scalable to wafer-sized cells and be useful for similar optoelectronic devices such as photodetectors.

References and Notes

1. W. U. Huynh, J. J. Dittmer, A. P. Alivisatos, *Science* **295**, 2425 (2002).
2. B. O'Regan, M. Grätzel, *Nature* **353**, 737 (1991).
3. A. Polman, H. A. Atwater, *Nat. Mater.* **11**, 174 (2012).
4. T. Mårtensson *et al.*, *Nano Lett.* **4**, 1987 (2004).
5. C. Colombo, M. Heiß, M. Grätzel, A. Fontcuberta i Morral, *Appl. Phys. Lett.* **94**, 173108 (2009).
6. J. F. Wang, M. S. Gudiksen, X. Duan, Y. Cui, C. M. Lieber, *Science* **293**, 1455 (2001).
7. M. T. Borgström *et al.*, *IEEE J. Sel. Top. Quantum Electron.* **17**, 1050 (2011).
8. E. C. Garnett, M. L. Brongersma, Y. Cui, M. D. McGehee, *Annu. Rev. Mater. Res.* **41**, 269 (2011).
9. H. Goto *et al.*, *Appl Phys Express* **2**, 035004 (2009).
10. J. Kupec, R. L. Stoop, B. Witzigmann, *Opt. Express* **18**, 27589 (2010).
11. L. Hu, G. Chen, *Nano Lett.* **7**, 3249 (2007).
12. N. Anttu, H. Q. Xu, *J. Nanosci. Nanotechnol.* **10**, 7183 (2010).
13. M. D. Kelzenberg *et al.*, *Nat. Mater.* **9**, 368 (2010).
14. E. Garnett, P. D. Yang, *Nano Lett.* **10**, 1082 (2010).
15. C. J. Keavney, V. E. Haven, S. M. Vernon, in *Photovoltaic Specialists Conference, 1990, Conference Record of the Twenty First IEEE* (IEEE, Piscataway, NJ, 1990), vol. 1, pp. 141–144.
16. M. A. Green, K. Emery, Y. Hishikawa, W. Warta, E. D. Dunlop, *Prog. Photovolt. Res. Appl.* **20**, 606 (2012).
17. M. T. Borgström *et al.*, *Nano Research* **3**, 264 (2010).
18. T. Mårtensson *et al.*, *Nano Lett.* **4**, 699 (2004).
19. See supplementary materials on *Science* Online.
20. N. Anttu, H. Q. Xu, *Phys. Rev. B* **83**, 165431 (2011).
21. P. M. Wu, N. Anttu, H. Q. Xu, L. Samuelson, M. E. Pistol, *Nano Lett.* **12**, 1990 (2012).
22. S. Münch *et al.*, *Nanotechnology* **21**, 105711 (2010).
23. H. J. Joyce *et al.*, *Nano Lett.* **12**, 5325 (2012).
24. A. Mishra *et al.*, *Appl. Phys. Lett.* **91**, 263104 (2007).
25. O. J. Glembocki, H. Piller, in *Handbook of Optical Constants of Solids*, E. D. Palik, Ed. (Academic Press, Orlando, FL, 1985), pp. 503–516.
26. M. H. M. van Weert *et al.*, *Appl. Phys. Lett.* **88**, 043109 (2006).
27. A. Yella *et al.*, *Science* **334**, 629 (2011).
28. A. H. Ip *et al.*, *Nat Nano* **7**, 577 (2012).

Acknowledgments: This work was performed within the Nanometer Structure Consortium at Lund University (nmC@LU) and was supported by the Swedish Research Council (Vetenskapsrådet), by the Knut and Alice Wallenberg Foundation, by the Swedish Energy Agency, and by the European Union program AMON-RA (214814). This Report is based on a project that was funded by E.ON AG as part of the E.ON International Research Initiative. We thank M. Graczyk for nanoimprint lithography and S. Lehmann for transmission electron microscopy.

Supplementary Materials

www.sciencemag.org/cgi/content/full/science.1230969/DC1
Materials and Methods
Figs. S1 to S3
Table S1
References (*29*–*33*)

1 October 2012; accepted 17 December 2012
Published online 17 January 2013;
10.1126/science.1230969

Synchronous Change of Atmospheric CO_2 and Antarctic Temperature During the Last Deglacial Warming

F. Parrenin,[1]* V. Masson-Delmotte,[2] P. Köhler,[3] D. Raynaud,[1] D. Paillard,[2] J. Schwander,[4] C. Barbante,[5,6] A. Landais,[2] A. Wegner,[3]† J. Jouzel[2]

Understanding the role of atmospheric CO_2 during past climate changes requires clear knowledge of how it varies in time relative to temperature. Antarctic ice cores preserve highly resolved records of atmospheric CO_2 and Antarctic temperature for the past 800,000 years. Here we propose a revised relative age scale for the concentration of atmospheric CO_2 and Antarctic temperature for the last deglacial warming, using data from five Antarctic ice cores. We infer the phasing between CO_2 concentration and Antarctic temperature at four times when their trends change abruptly. We find no significant asynchrony between them, indicating that Antarctic temperature did not begin to rise hundreds of years before the concentration of atmospheric CO_2, as has been suggested by earlier studies.

Analyses of polar ice cores have shown that the concentration of atmospheric CO_2 (aCO_2) and surface air temperature are closely related and that they have risen and fallen in tandem over most of the past 800,000 years. However, whether changes of temperature occurred first and how large that lead may have been have been topics of considerable controversy. The most highly resolved aCO_2 record during the last deglacial warming, Termination I (TI), is from the European Project for Ice Coring in Antarctica (EPICA) Dome C (EDC) ice core (*1*, *2*). In this record, aCO_2 appears to lag local Antarctic temperature (AT) by 800 ± 600 years at the onset of TI, in agreement with an earlier study on the Vostok and Taylor Dome ice cores, which identified a lag of 600 ± 400 years at the end of the

[1]Laboratoire de Glaciologie et Géophysique de l'Environnement (CNRS/UJF), Grenoble, France. [2]Laboratoire des Sciences du Climat et de l'Environnement (CEA/CNRS/UVSQ-IPSL), Gif-sur-Yvette, France. [3]Alfred Wegener Institute for Polar and Marine Research, Bremerhaven, Germany. [4]Physics Institute, University of Bern, Bern, Switzerland. [5]Department of Environmental Sciences, University of Venice, Venice, Italy. [6]Institute for the Dynamics of Environmental Processes–CNR, University of Venice, Venice, Italy.

*Corresponding author. E-mail: parrenin@ujf-grenoble.fr
†Present address: Byrd Polar Research Center, Ohio State University, Columbus, OH, USA.

past three terminations (*3*). However, uncertainties in the relative timing of aCO_2 and AT remain for two reasons. First, air is trapped in fallen snow only when it has recrystallized enough to create enclosed cavities, typically at a depth of 50 to 120 m below the surface (depending on site conditions), at the bottom of the so-called firn. This results in a depth difference (Δdepth, see Fig. 1) between synchronous events recorded in the ice matrix and in the trapped gas bubbles or hydrates (*4*, *5*). We used air $\delta^{15}N$ data from the EDC ice core to determine the past Lock-In Depth (LID), which is the depth at which air in the ice is permanently trapped. The LID estimates are transformed to Δdepth estimates, using a constant firn average density and a modeled vertical thinning function. Our approach is further validated with two independent methods. Second, using only the isotopic record from one ice core produces a noisy reconstruction of past temperature variations in Antarctica. We used a stack of AT variations based on five synchronized ice cores.

Figure 2 illustrates an approach similar to previous studies (*1*, *3*) to deduce Δdepth, based on firn densification modeling (*6*) to estimate the past LID and average firn density, and on ice flow modeling (*7*) to estimate the vertical thinning of ice layers. The past LID can also be estimated using the fact that in the firn, below a convective zone where the air is freely mixed, gravitational fractionation enriches the $\delta^{15}N$ of N_2 proportionally to the height of the diffusive column (*8*, *9*). There is no convective zone today at EDC (*10*). Assuming a persistent absence of such a convective zone during TI and using the $\delta^{15}N$ data from the EDC ice core (*11*), we can estimate the LID during TI. Then, assuming that the average firn density did not vary and using a one-dimensional ice flow model (*7*) to assess layer thinning, the LID can be converted to Δdepth (Fig. 2 and supplementary materials).

One caveat of our method arises from our assumption of the absence of a convective zone during the past, which is known to reach more than 20 m in low-accumulation windy sites today (*12*). For verification, we used two independent approaches. First, we synchronized EDC to the EPICA Dronning Maud Land (EDML) and Talos Dome (TALDICE) ice cores both in the gas (using CH_4) and ice (using volcanic events) phases (*5*). The Δdepth at EDC can be estimated from Δdepth at EDML and TALDICE (Fig. 1). The latter is evaluated from firn modeling but, because the accumulation is about three times higher at EDML or TALDICE than at EDC, an error on the past LID at EDML or TALIDCE has an impact at EDC that is about three times smaller (*5*). Second, we used the bipolar seesaw hypothesis (*13*), which suggests that a rapid temperature rise in Greenland occurs synchronous to a maximum in AT, and a rapid temperature fall occurs synchronous to a minimum. This hypothesis has been proven by relative dating of ice cores around the Laschamp geomagnetic event (*14*).We assumed that the fast CH_4 transitions in EDC can be taken as proxies of rapid Greenland temperature changes, thus revealing three tie points during TI (Fig. 3). The fact that it is possible, with a very simple mathematical model (*15*), to construct from the EDC ice isotope record a Greenland-like temperature time-series, correctly capturing stadial-interstadial transitions (corresponding to the extrema of the EDC ice isotope record) makes it very likely that the bipolar seesaw pattern is robust during these rapid transitions. These independent methods, either based on the synchronization of EDC to EDML and TALDICE or on the bipolar seesaw hypothesis, confirm our $\delta^{15}N$ method for TI within their 1σ confidence intervals, suggesting that the convective zone indeed was absent or nearly absent during TI at EDC.

We therefore built a new gas chronology based on filtered $\delta^{15}N$ data (supplementary materials). The reason why we based our new gas chronology only on the $\delta^{15}N$ method is twofold. First, the $\delta^{15}N$ method allows us to produce a continuous gas age scale along TI, whereas the other two methods give only three tie points (at times when CH_4 varies abruptly: the onset of the Bølling oscillation, the onset of the Younger Dryas, and the onset of the Holocene) and in particular cannot provide constraints for the onset of TI. Second, apart from the zero–convective-zone assumption, the $\delta^{15}N$ method has the smallest analytical uncertainty (Fig. 2).

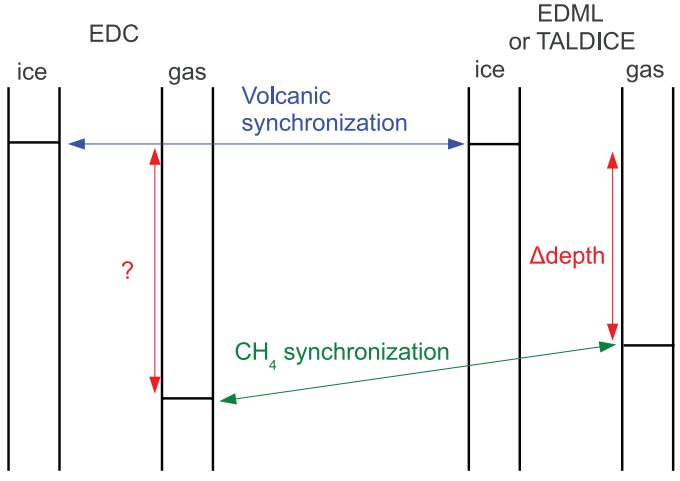

Fig. 1. Scheme illustrating the deduction of Δdepth at EDC from ice (volcanic) and gas (CH_4) synchronization to the EDML or TADLICE ice cores and evaluation of Δdepth at EDML or TALDICE.

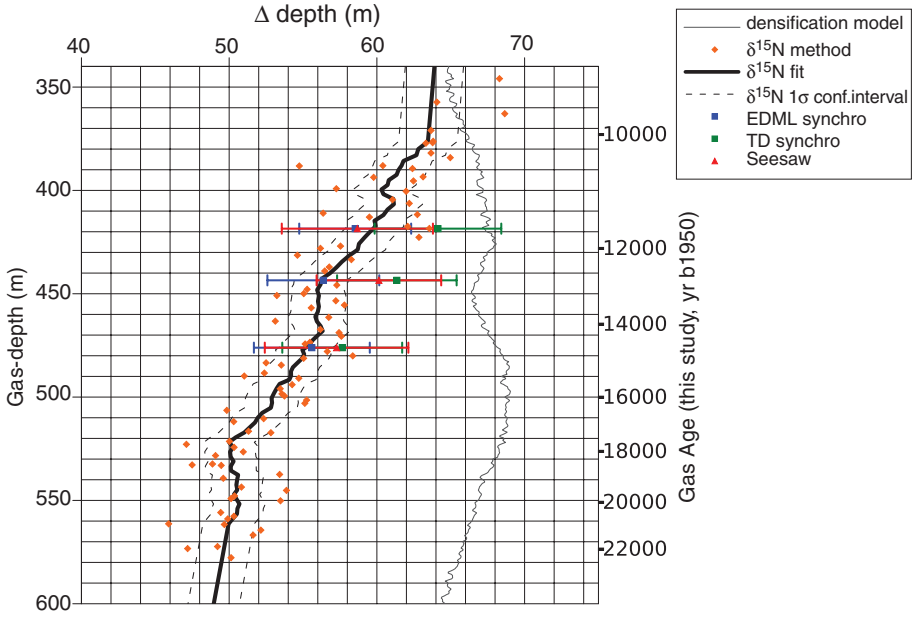

Fig. 2. Estimation of Δdepth along the EDC ice core using different methods: purely based on modeling (densification and ice flow, gray line), based on $\delta^{15}N$ data and ice flow modeling (orange dots), based on the synchronization to the EDML ice core (blue square), based on synchronization to the TALDICE ice core (green square), or based on the bipolar seesaw hypothesis (red triangle). The black line is a fit (supplementary materials) to the $\delta^{15}N$ estimates, and the dashed lines represent its 1σ confidence interval. The estimation of 1σ uncertainties is described in (*5*) and in the supplementary materials. yr b1950, years before 1950.

The three approaches—$\delta^{15}N$, synchronization to EDML and TALDICE, and seesaw methods—all disagree with the firn densification model simulation for EDC (Fig. 2), which probably lacks important processes affecting densification under glacial conditions, such as the effect of increased concentrations of impurities (*16*).

A second step to examine the phasing between aCO_2 and AT during TI is to produce an accurate record of AT during the past [an Antarctic Temperature Stack (ATS)]. To do this, we stacked (supplementary materials) the isotopic temperature reconstructions from five different ice cores (EDC, Vostok, Dome Fuji, TALDICE, and EDML) after the synchronization of these ice cores to the EDC record. This stacking process considerably reduces the noise in comparison to the single EDC record (Fig. 4): The standard deviation of ATS to its 220-year moving average is 0.20°C, whereas it is 0.52°C for the EDC temperature record (with both ATS and the EDC temperature record being resampled every 20 years).

The temporal variations of aCO_2 and AT across TI (Fig. 4) on our chronology are highly correlated (Pearson correlation coefficient of 0.993 for a 20-year resampled time series). Both records can be accurately fitted by a six-point linear function (Fig. 4 and supplementary materials). We infer the aCO_2-AT phasing at the four break points using a Monte-Carlo algorithm (supplementary materials): the onset of TI (10 ± 160 years, 1σ, aCO_2 leads), the onset of the Bølling oscillation (–260 ± 130 years, AT leads), the onset of the Younger Dryas (60 ± 120 years, aCO_2 leads), and the onset of the Holocene (–500 ± 90 years, AT leads). The uncertainty takes into account the uncertainty in the determination of the break points and the uncertainty in the determination of Δdepth. The only significant aCO_2-AT lags are observed at the onsets of the Bølling oscillation and the Holocene. It should be noted that during these two events, the associated sharp increases in aCO_2 were probably larger and more abrupt than the signals recorded in the ice core, due to the diffusion in the gas recording process (*17*). This atmosphere–ice core difference biases our break point determination toward younger ages. If we use these fast increases to determine the break points in aCO_2, we find a lag of –10 ± 130 years (1σ) for the Bølling onset and –130 ± 90 years (1σ) for the Holocene onset; that is, no significant phasing. If, instead of using aCO_2 we use the radiative forcing of aCO_2 (*18*) [$rCO_2 = 5.35\ W/m^2\ \ln(CO_2/280$ parts per million by volume)], the inferred phasing is not significantly changed (Fig. 4).

Our evaluation of the aCO_2-AT phasing for TI differs from the 800 ± 200 year (lead of AT) estimate for TIII (*19*), based on the hypothesis that $\delta^{40}Ar$ of air is a gas proxy for local temperature. We cannot exclude the possibility that the aCO_2-AT phasing is different for TI and TIII. However, if as recently suggested (*16*) the LID is influenced by the impurity content of the firn, $\delta^{40}Ar$, which, as $\delta^{15}N$, follows a gravitational

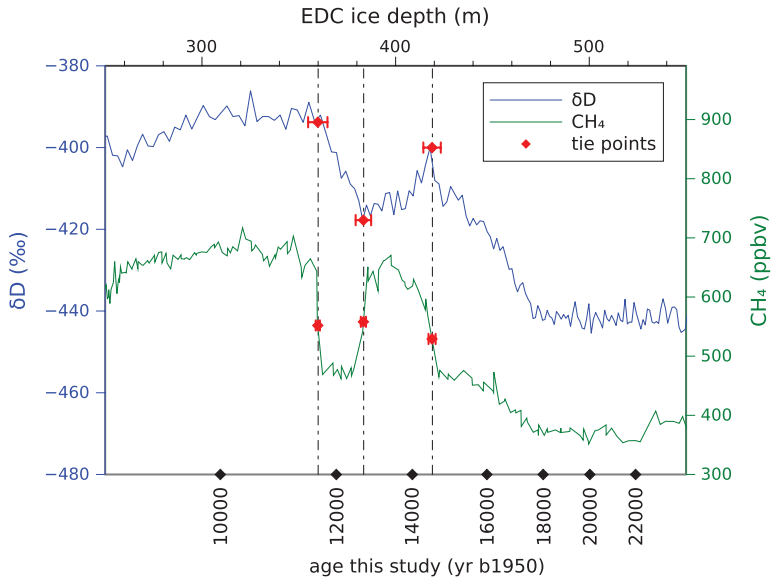

Fig. 3. The bipolar seesaw hypothesis allows us to derive three Δdepth estimates at EDC during the last deglacial warming, using the 100-year resampled δD record (*28*) and the CH_4 record (*29*). Error bars on the depths of tie points are 1σ. The EDC gas depth scale is linearly stretched according to the tie points.

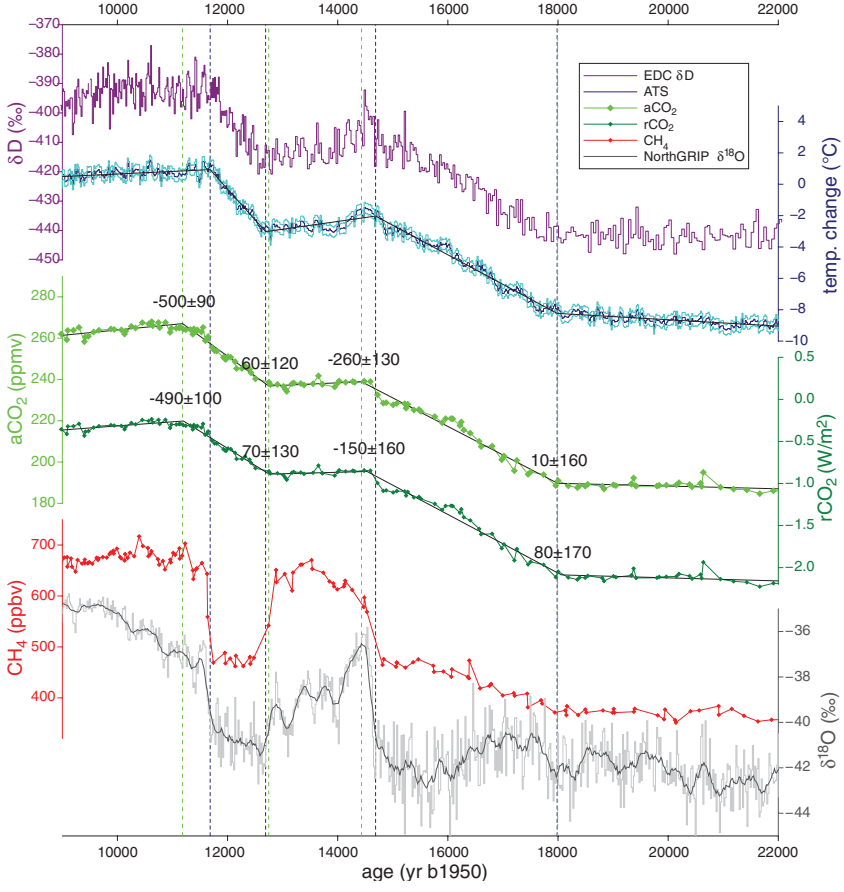

Fig. 4. Various climate time series during TI. Shown are δD from EDC (*28*) (purple), ATS (dark blue, this study) and confidence interval (light blue), aCO_2 from EDC (*1*, *2*) (light green), rCO_2 (dark green), atmospheric CH_4 from EDC (*29*) (red), and Greenland $\delta^{18}O$ from NorthGRIP (gray) onto the GICC05 age scale (*27*) with a 220-year running average (dark gray). The solid lines represent the best six-point linear fit of ATS, aCO_2, and rCO_2 (supplementary materials). The vertical dashed lines mark the four break points in ATS (blue) and in aCO_2 (green), where we evaluated the aCO_2-AT and the rCO_2-AT phase lags (black numbers). The new EDC age scale is described in the supplementary materials.

enrichment, should be paced by changes in dust concentration. During TIII, the change in dust occurs earlier than the change in ice isotope at both EDC and Vostok (figs. S7 and S8), whereas these two records are approximately in phase during TI (fig. S8). This could explain why the Vostok $\delta^{40}Ar$ record is in advance with respect to the aCO_2 record, without contradicting our finding of synchronous changes in aCO_2 and AT. During TII at EDC (fig. S8), on the other hand, the change in $\delta^{15}N$ occurs at a deeper depth than the change in dust. Dust concentration therefore cannot be the only factor influencing the LID.

Our results are also in general agreement with a recent 0- to 400-year aCO_2-AT average lag estimate for TI (*20*), using a different approach. Although this study does not make any assumption about the convective zone thickness, it is based on coastal cores, which might be biased by local changes in ice sheet thickness; and firn densification models, which may not be valid for past conditions (see the supplementary materials for a more detailed discussion).

Our chronology and the resulting aCO_2-AT phasing strengthens the hypothesis that there was a close coupling between aCO_2 and AT on both orbital and millennial time scales. The aCO_2 rise could contribute to much of the AT change during TI, even at its onset, accounting for positive feedbacks and polar amplification (*21*), which magnify the impact of the relatively weak rCO_2 change (Fig. 4) that alone accounts for ~0.6°C of global warming during TI (*21*). Invoking changes in the strength of the Atlantic meridional overturning circulation is no longer required to explain the lead of AT over aCO_2 (*22*).

Given the importance of the Southern Ocean in carbon cycle processes (*23*), one should not exclude the possibility that aCO_2 and AT are interconnected through another common mechanism such as a relationship between sea ice cover and ocean stratification. Although the tight link between aCO_2 and AT suggests a major common mechanism, reviews of carbon cycle processes suggest a complex association of numerous independent mechanisms (*2*, *23*).

Changes in aCO_2 and AT were synchronous during TI within uncertainties. Our method, based on air ^{15}N measurements to determine the ice/gas depth shift, is currently being used in the construction of a common and optimized chronology for all Antarctic ice cores (*24*, *25*). The assumption that no convective zone existed at EDC during TI might be tested in the future by using Kr and Xe isotopes (*26*). Further studies on the firn are needed to understand the causes of the past variations of the LID, such as the possible impact of impurity concentrations on the densification velocity. Although our study was focused on the relative timing of TI climatic records extracted from Antarctic ice cores, there is now the need to build a global chronological framework for greenhouse gases, temperature reconstructions, and other climate proxies at various locations (*22*). Although the timings of the Bølling, Younger Dryas, and Holocene onsets as visible in the methane records are now well constrained by a layer-counted Greenland chronology (*27*), determining the timing of the onset of TI in Antarctic records remains challenging. Modeling studies using coupled carbon cycle–climate models will be needed to fully explore the implications of this synchronous change of AT and aCO_2 during TI in order to improve our understanding of natural climate change mechanisms.

References and Notes

1. E. Monnin *et al.*, *Science* **291**, 112 (2001).
2. A. Lourantou *et al.*, *Global Biogeochem. Cycles* **24**, GB2015 (2010).
3. H. Fischer, M. Wahlen, J. Smith, D. Mastroianni, B. Deck, *Science* **283**, 1712 (1999).
4. L. Loulergue *et al.*, *Clim. Past* **3**, 527 (2007).
5. F. Parrenin *et al.*, *Clim. Past* **8**, 1239 (2012).
6. C. Goujon, J.-M. Barnola, C. Ritz, *J. Geophys. Res.* **108**, ACL10/1-10 (2003).
7. F. Parrenin *et al.*, *Clim. Past* **3**, 243 (2007).
8. H. Craig, Y. Horibe, T. Sowers, *Science* **242**, 1675 (1988).
9. T. A. Sowers, M. Bender, D. Raynaud, Y. L. Korotkevich, *J. Geophys. Res.* **97**, 15683 (1992).
10. A. Landais *et al.*, *Quat. Sci. Rev.* **25**, 49 (2006).
11. G. B. Dreyfus *et al.*, *Quat. Sci. Rev.* **29**, 28 (2010).
12. J. P. Severinghaus *et al.*, *Earth Planet. Sci. Lett.* **293**, 359 (2010).
13. T. F. Stocker, S. J. Johnsen, *Paleoceanography* **18**, 1 (2003).
14. G. M. Raisbeck, F. Yiou, J. Jouzel, T. F. Stocker, *Clim. Past* **3**, 541 (2007).
15. S. Barker *et al.*, *Science* **334**, 347 (2011).
16. M. Hörhold *et al.*, *Earth Planet. Sci. Lett.* **325–326**, 93 (2012).
17. P. Köhler, G. Knorr, D. Buiron, A. Lourantou, J. Chappellaz, *Clim. Past* **7**, 473 (2011).
18. G. Myhre, E. J. Highwood, K. P. Shine, F. Stordal, *Geophys. Res. Lett.* **25**, 2715 (1998).
19. N. Caillon *et al.*, *Science* **299**, 1728 (2003).
20. J. B. Pedro, S. O. Rasmussen, T. D. van Ommen, *Clim. Past* **8**, 1213 (2012).
21. P. Köhler *et al.*, *Quat. Sci. Rev.* **29**, 129 (2010).
22. J. D. Shakun *et al.*, *Nature* **484**, 49 (2012).
23. H. Fischer *et al.*, *Quat. Sci. Rev.* **29**, 193 (2010).
24. L. Bazin *et al.*, *Clim. Past Discuss.* **8**, 5963 (2012).
25. D. Veres *et al.*, *Clim. Past Discuss.* **8**, 6011 (2012).
26. J. P. Severinghaus, A. Grachev, B. Luz, N. Caillon, *Geochim. Cosmochim. Acta* **67**, 325 (2003).
27. A. Svensson *et al.*, *Clim. Past* **4**, 47 (2008).
28. J. Jouzel *et al.*, *Science* **317**, 793 (2007).
29. L. Loulergue *et al.*, *Nature* **453**, 383 (2008).

Acknowledgments: We thank O. Watanabe, B. Stenni, and EPICA community members for giving access to, respectively, the DF1, TALDICE, and EDML isotopic data; L. Loulergue, D. Buiron, and T. Blunier for giving access to, respectively, the EDC-EDML, TALDICE, and GRIP CH_4 data; G. Dreyfus for giving access to the $\delta^{15}N$ isotopic data; and G. Delaygue, J. Chappellaz, S. Barker, and A. Ganopolski for helpful discussions. This work greatly benefited from constructive comments by two anonymous reviewers. This work had support from the French Agence Nationale de la Recherche (project ANR-07-BLAN-0125 "Dome A" and ANR-09-SYSC-001 "ADAGE"). This work is a contribution to EPICA, a joint European Science Foundation/European Commission scientific program, funded by the European Union and by national contributions from Belgium, Denmark, France, Germany, Italy, the Netherlands, Norway, Sweden, Switzerland, and the United Kingdom. Main logistical support was provided by the Institut Paul Emile Victor and the Programma Nazionale Ricerche in Antartide at Dome C. We thank the technical teams in the field and at the different laboratories. This is EPICA publication no. 291.

Supplementary Materials

www.sciencemag.org/cgi/content/full/339/6123/1060/DC1
Materials and Methods
Supplementary Text
Figs. S1 to S8
Tables S1 to S7
Database S1

20 June 2012; accepted 9 January 2013
10.1126/science.1226368

Genomic Diversity and Evolution of the Head Crest in the Rock Pigeon

Michael D. Shapiro,[1]* Zev Kronenberg,[2] Cai Li,[3,4] Eric T. Domyan,[1] Hailin Pan,[3] Michael Campbell,[2] Hao Tan,[3] Chad D. Huff,[2,5] Haofu Hu,[3] Anna I. Vickrey,[1] Sandra C. A. Nielsen,[4] Sydney A. Stringham,[1] Hao Hu,[5] Eske Willerslev,[4] M. Thomas P. Gilbert,[4,6] Mark Yandell,[2] Guojie Zhang,[3] Jun Wang[3,7,8]*

The geographic origins of breeds and the genetic basis of variation within the widely distributed and phenotypically diverse domestic rock pigeon (*Columba livia*) remain largely unknown. We generated a rock pigeon reference genome and additional genome sequences representing domestic and feral populations. We found evidence for the origins of major breed groups in the Middle East and contributions from a racing breed to North American feral populations. We identified the gene *EphB2* as a strong candidate for the derived head crest phenotype shared by numerous breeds, an important trait in mate selection in many avian species. We also found evidence that this trait evolved just once and spread throughout the species, and that the crest originates early in development by the localized molecular reversal of feather bud polarity.

Since the initial domestication of the rock pigeon in Neolithic times (*1*), breeders have selected striking differences in behavior, vocalizations, skeletal morphology, feather ornaments, colors, and color patterns to establish over 350 breeds (*2*). In many cases, the number and magnitude of differences among breeds are more characteristic of macroevolutionary changes than of changes within a single species (*2*, *3*). Indeed, Charles Darwin was so fascinated by domestic pigeons that he repeatedly called attention to this dramatic example of diversity within a species to communicate his ideas about natural selection (*3*, *4*).